Proceedings of the ASME 2016 International Design Engineering Technical Conferences & Design Automation Conference
IDETC/DAC 2016
August 21-24, 2016, Charlotte, North Carolina, USA

IDETC2016-60096

DESIGN OPTIMIZATION AND ANALYSIS OF A PRESCRIBED VIBRATION SYSTEM

Bongani Malinga
North Carolina State University
Raleigh, North Carolina, 27695
bmaling@ncsu.edu

Scott M. Ferguson
North Carolina State University
Raleigh, North Carolina, 27695
scott_ferguson@ncsu.edu

Gregory D. Buckner
North Carolina State University
Raleigh, North Carolina, 27695
greg_buckner@ncsu.edu

ABSTRACT

Advances in technology that come with increased system complexity have accentuated the intricacy of decision making in engineering design. This has stimulated a great deal of research in ways to incorporate decision analysis and multi-attribute decision-making theory in engineering problems. In this research, Conjoint Value Analysis is incorporated into a scheme that optimizes the design of a multi-attribute Prescribed Vibration System. The influence of designer preferences is investigated by comparing design alternatives that result from different preference rankings. Monte Carlo-based uncertainty and sensitivity studies are performed to support the design process by providing additional information on the candidate designs. By understanding how small changes in the values of optimized parameters influence the system attributes, sensitivity analysis and uncertainty analyses can be used as a design robustness measure. The overall choice of the design is therefore based not only on the performance objectives but also on the resulting system robustness, which is very valuable considering manufacturing variations and tolerance stacks.

1 INTRODUCTION

Technological advances that introduce increased system complexity can add significant uncertainty to design parameters, boundary conditions and system behavior. The Prescribed Vibration System presented in [1] is one such example and provides the basis for the work presented in this paper. Sources of uncertainty in this system include manufacturing variations, design imprecision, errors in inertial approximations and structural irregularities. While there are ways of quantifying these errors and reducing them, they are impossible to eliminate. Design decisions still have to be made in the face of risky and uncertain system performance. The realization that making decisions is an intricate part of engineering design has stimulated a great deal of research in areas of solution space exploration [2], data variability [3], decision analysis and multi-attribute decision making [4] [5]. The main goal of a decision-making process is improving decision quality and creating reliable and profitable products [6]. Techniques that incorporate designer preferences coupled with uncertainty studies can be used in product development to help accomplish this goal.

Advanced uncertainty analysis methods can be used to accurately quantify and propagate uncertainties in engineering design problems. A common uncertainty analysis technique uses a probabilistic approach, which assumes known probability density function (pdf) information. The benefit of probabilistic analysis is the ability to produce comprehensive results, instead of a single result based on the mean design point. These probabilistic techniques have been successfully used in many applications such as bridge failure assessment, multi-criteria decision analysis and reliability of steel connections [7], [8], [9]. In addition, it has been shown that incorporating uncertainty-based analysis and / or reliability-based design can provide risk reduction by accounting for various uncertainties in the design process [10]. It is, therefore, essential for the overall design choice to be based not only on the performance objectives but also on the resulting system robustness. This is very valuable, considering the uncertainties that can result from manufacturing variations and tolerance stacks.

This paper builds on the work presented in [1] where Conjoint Value Analysis (CVA) [11] was used to optimize the design of a Prescribed Vibration System (PVS). The current work reformulates the dynamic model of the system attributes and focuses on characterizing and understanding the uncertainty and sensitivity of the resulting PVS designs. Monte Carlo-based uncertainty and sensitivity studies are performed to support the design process by providing additional information on the candidate designs. By understanding how small changes in the optimized design parameters influence the system attributes, sensitivity analysis and uncertainty analyses can be used as a design robustness measure. An uncertainty analysis describes the entire set of possible outcomes, together with their associated occurrence probabilities. A sensitivity analysis determines the changes in system output values that result from modest changes within a localized region of the design parameter space.

The remainder of the paper is organized as follows; the next section presents the prescribed vibration system dynamic models and the preference-based multi-attribute optimization scheme. It then examines Monte Carlo-based uncertainty and sensitivity analyses as a way to quantify the relative robustness of alternative designs to design parameter imprecision. Simulation and results are then presented, followed by conclusions and future work.

2 SYSTEM OVERVIEW

The PVS comprises: (1) actuators, also referred to as circular force generators. These are motorized eccentric rotors implemented in proximal pairs that enable the production of controllable rotating forces, (2) accelerometers affixed to the shale shaker structure for measuring the vibration profiles, and (3) a controller that monitors these sensors and regulates actuator force magnitudes and phases to achieve and maintain a prescribed vibration profile. The system is intended for installation on shale shakers [12] that mechanically filter solids from fluids in oil and gas drilling operations. Figure 1 shows the control and optimization loops associated with the design of the PVS. In the control loop, the user-specified vibration profile is converted to a time-domain reference acceleration a_r, which is compared to the measured acceleration a_m to determine the acceleration tracking error a_e. A feedforward controller regulates the actuator control forces to minimize a_e.

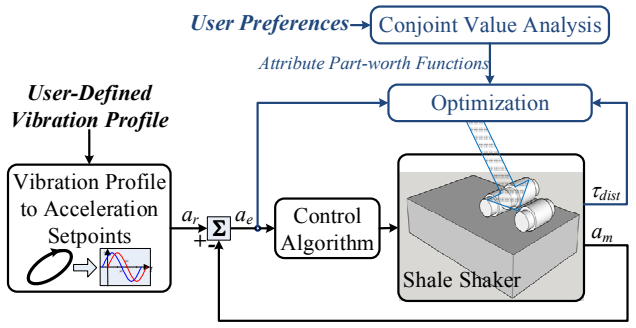

Figure 1: PVS block diagram showing the control and optimization loops.

The acceleration error a_e also serves as the basis for the "performance" system attributes $f_1(X)$ and $f_2(X)$, that measure how closely the vibration profile tracks the desired profiles for a specific vector of design parameters X. Another system attribute, the "efficiency" attribute $f_3(X)$, quantifies the power required to achieve a given performance. The optimization loop determines optimal actuator placement by minimizing a weighted objective function, formulated using Conjoint Value Analysis (CVA). An overview of the modeling and optimization methods are presented in subsequent sections. Details can be found in [1].

2.1 VIBRATION PROFILE DEFINITION

The acceleration at location k (where $k = 1, 2, 3$ corresponds to the shale shaker entrance, interior and exit, respectively) can be generalized by considering a typical elliptical vibration profile oriented at angle α with major axis acceleration A_m and minor acceleration rA_m, where r is the ellipse ratio. Figure 2 illustrates the ellipse properties and the associated time history plots.

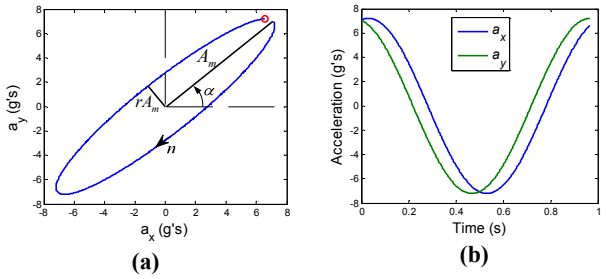

Figure 2: General vibration profile showing (a) x vs. y-axis elliptical vibration (b) x and y-axis acceleration time histories

Based on the user-specified vibration profile, the x-axis and y-axis accelerations at location k can be expressed as:

$$a_{xk} = A_{xk}\cos(n_k\omega t + \phi_{xk})$$
$$a_{yk} = A_{yk}\cos(n_k\omega t + \phi_{yk}) \quad (1)$$

where A_{xk}, A_{yk} are the acceleration magnitudes and ϕ_{xk}, ϕ_{yk} are the respective acceleration phase offsets with respect to a global reference angle ωt. n_k specifies the rotational direction of the ellipse with, $n_k = +1$ for counter-clockwise rotation (as illustrated) and $n = -1$ for clockwise rotation. Using elliptical motion equations, the acceleration magnitudes are given by

$$A_{xk} = A_{mk}\sqrt{r^2\sin^2(\alpha) + \cos^2(\alpha)}$$
$$A_{yk} = A_{mk}\sqrt{\sin^2(\alpha) + r^2\cos^2(\alpha)} \quad (2)$$

and the acceleration phases are given by

$$\phi_{xk} = \tan^{-1}(r/\tan(\alpha))$$
$$\phi_{yk} = \tan^{-1}(-r/\tan(\alpha)) \quad (3)$$

Considering the shale shaker as a rigid body, the user only needs to specify the profile characteristics (A_m, r, α) for location 1. A progressive vibration profile [12], [1] can be achieved by defining an additional parameter β, a measure of acceleration progression that correlates to the shale shaker's angular acceleration $\dot{\omega}_{cg}$. The control problem can then be solved by considering the acceleration at location 1 and the angular acceleration, resulting in the reference vector $a_r = [a_{x1}, a_{y1}, \dot{\omega}_{cg}]$. Furthermore, the acceleration magnitudes and phases can be geometrically represented as a complex pair of static accelerations. Thus, the acceleration reference vector can be represented as

$$a_r = [\mathrm{re}, \mathrm{im}(a_{x\_sp1}), \mathrm{re}, \mathrm{im}(a_{x\_sp1}), \mathrm{re}, \mathrm{im}(\dot{\omega}_{sp\_cg})]^T \quad (4)$$

2.2 PVS MODEL

Figure 3 shows a schematic of the screen basket (the vibrating portion of the shale shaker) with mass M and mass moment of inertia about the z-axis J_z, outfitted with i actuators. Each actuator, located at $[x_i, y_i]$, produces a net force F_i that rotates at a regulated angular speed ω in direction n_i. This rotating force has a phase offset Φ_i relative to the global reference. This force is controlled by the relative phasing of rotating eccentric masses m_{i1} and m_{i2} located at radius r. These i forces combine to produce the screen basket response, quantified by $[a_{x\_cg}, a_{y\_cg}]$ and $\dot{\omega}_{cg}$, the respective linear and angular accelerations at the screen basket center of gravity (cg) located at $[x_{cg}, y_{cg}]$. The resulting acceleration measurement $[a_{y\_mk}, a_{y\_mk}]$ at location k with coordinates $[x_{mk}, y_{mk}]$ can be determined by analyzing the screen basket dynamics.

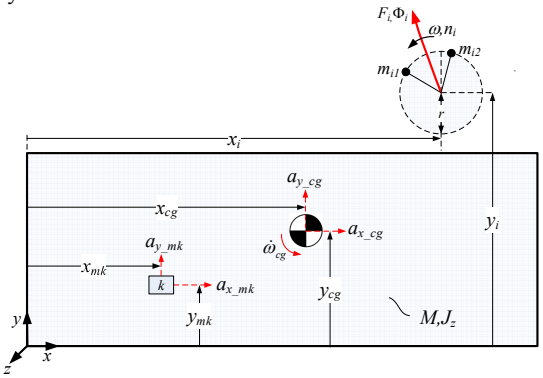

Figure 3: Screen basket outfitted with *i* actuators to create the desired vibration profile at measurement location *k*.

For any steady-state vibration condition, the steady-state linear and angular accelerations can be expressed as functions of the static actuator force amplitudes and phases F_i and Φ_i, respectively. The time-dependent trigonometric terms can be geometrically mapped to the complex plane, where the cosine and sine terms are considered real and imaginary, respectively. The resulting model is a complex-valued matrix that quantifies the linear and angular accelerations at the screen basket center of gravity.

$$\begin{bmatrix} \mathrm{re}(a_{x\_cg}) \\ \mathrm{im}(a_{x\_cg}) \\ \mathrm{re}(a_{y\_cg}) \\ \mathrm{im}(a_{y\_cg}) \\ \mathrm{re}(\dot{\omega}_{cg}) \\ \mathrm{im}(\dot{\omega}_{cg}) \end{bmatrix} = \begin{bmatrix} 1/m & 0 & \cdots & 1/m & 0 \\ 0 & n_i/m & & 0 & n_i/m \\ 0 & 1/m & & 0 & 1/m \\ n_1 & 0 & \cdots & n_i & 0 \\ -\frac{(y_1-y_{cg})}{J_z} & \frac{(x_1-x_{cg})}{J_z} & & -\frac{(y_i-y_{cg})}{J_z} & \frac{(x_i-x_{cg})}{J_z} \\ \frac{(x_1-x_{cg})n_i}{J_z} & \frac{(y_1-y_{cg})n_i}{J_z} & & \frac{(x_i-x_{cg})n_i}{J_z} & \frac{(y_i-y_{cg})n_i}{J_z} \end{bmatrix} \begin{Bmatrix} a_1 \\ b_1 \\ \vdots \\ a_i \\ b_i \end{Bmatrix} \quad (5)$$

where $a_i = F_i \cos(\Phi_i)$ and $b_i = F_i \sin(\Phi_i)$.

This model reflects that the screen basket response is a linear sum of the responses caused by each of the n actuators. The net screen basket acceleration can be calculated based on the cross product of angular acceleration and offset distances of all n actuators.

$$a_m = \begin{bmatrix} \mathrm{re}(a_{x\_m1}) \\ \mathrm{im}(a_{x\_m1}) \\ \mathrm{re}(a_{y\_m1}) \\ \mathrm{im}(a_{y\_m1}) \\ \mathrm{re}(\dot{\omega}_{cg}) \\ \mathrm{im}(\dot{\omega}_{cg}) \end{bmatrix} = \begin{bmatrix} \mathrm{re}(a_{x\_cg}) \\ \mathrm{im}(a_{x\_cg}) \\ \mathrm{re}(a_{y\_cg}) \\ \mathrm{im}(a_{y\_cg}) \\ \mathrm{re}(\dot{\omega}_{cg}) \\ \mathrm{im}(\dot{\omega}_{cg}) \end{bmatrix} + \begin{bmatrix} \mathrm{re}(\dot{\omega}_{cg}) \times (y_{m1} - y_{cg}) \\ \mathrm{im}(\dot{\omega}_{cg}) \times (y_{m1} - y_{cg}) \\ \mathrm{re}(\dot{\omega}_{cg}) \times (x_{m1} - x_{cg}) \\ \mathrm{im}(\dot{\omega}_{cg}) \times (x_{m1} - x_{cg}) \\ 0 \\ 0 \end{bmatrix} \quad (6)$$

Additionally, (6) can be used to quantify the complex acceleration $[a_{y\_mk}, a_{y\_mk}]$ at any measurement location k using appropriate sensor location coordinates. For details on the model derivation, the reader is referred to [1].

The system design vector X is defined as

$$X = [x_1, y_2, x_2, y_2 \ldots . x_n, y_n, \rho] \quad (7)$$

where, $x_1, y_2, x_2, y_2 \ldots . x_n, y_n$ is the actuator location vector (each x_1, y_2 pair represents and actuator location point) relative to any fixed reference point on the screen basket; ρ is the product of the actuator eccentric mass m and the fixed rotation radius r and it defines the actuator force capacity.

2.3 SYSTEM ATTRIBUTES

For any desired profile, the goal is to minimize the vibration magnitude error and the vibration angle error in a manner that minimizes required actuator power. Referring to the generic elliptical profile shown in Figure 2(a), the difference between $A_m|_r$ and $A_m|_m$, the respective reference and measured major axis accelerations, defines the vibration magnitude error $|\varepsilon|$. The difference between $\alpha|_r$ and $\alpha|_m$, the respective reference and measured major axis angles, defines the vibration angle error $\varepsilon_\angle$.

$$\begin{aligned} |\varepsilon|_k &= A_m|_{r_k} - A_m|_{m_k} \\ \varepsilon_{\angle_k} &= \alpha|_{r\_k} - \alpha|_{m\_k} \end{aligned} \qquad k = 1, 2, 3 \quad (8)$$

Ideally, the system should be designed in a manner that minimizes required actuator power, which can be quantified in terms of motor torque τ. This torque must account for gravitational forces, friction and damping effects, transient accelerations and disturbances associated with the motion of each actuator mounting base. During normal operating conditions, most of these torque components do not change significantly. However, the torque required to overcome base disturbances, referred to as the disturbance torque τ_{dist}, can vary in a way that significantly affects the total power requirement. For this reason, the "efficiency" system attribute $f_3(X)$ is defined to be a scalar metric of τ_{dist}.

For the j^{th} eccentric mass on the i^{th} on the actuator, the disturbance torque can be expressed as [1]

$$\tau_{dist\_dc\_ij} = \frac{1}{2}\rho_{ij}\left[A_y \cos(\phi_{yi} - \phi_{ij}) + A_x \sin(\phi_{xi} - \phi_{ij})\right] \quad (9)$$

where ϕ_{ij} is the phase angle of the eccentric mass motion relative to the global coordinate system and A_x, A_y and ϕ_{xi}, ϕ_{yi} are the x and y-axis acceleration magnitudes and phases respectively. For details on the derivation of the model, the reader is referred to [1].

2.3.1 PERFORMANCE

The "performance" system attributes $f_1(X)$ and $f_2(X)$ are defined to quantify system performance as a function of the design parameters X. In this implementation, $f_1(X)$ is the mean square error of the magnitude error $|\varepsilon|$ and $f_2(X)$ is the mean square error of the angle error $\varepsilon_\angle$ across the three shale shaker locations.

$$f_1(X) = \sqrt{\tfrac{1}{3}\textstyle\sum_1^3 |\varepsilon|_k^2} \quad (10)$$

$$f_2(X) = \sqrt{\tfrac{1}{3}\textstyle\sum_1^3 \varepsilon_{\angle_k}^2} \quad (11)$$

2.3.2 EFFICIENCY

The efficiency attribute $f_3(X)$ is the maximum value of the squared disturbance torques:

$$f_3(X) = max\left\{{\tau_{dist_{dc_{11}}}}^2, \ldots \ldots {\tau_{dist_{dc_{ij}}}}^2\right\};\ i = 1..n;\ j = 1,2 \quad (12)$$

3 METHODS

3.1 CONJOINT VALUE ANALYSIS

Conjoint Value Analysis (CVA) is a method used in marketing research to quantitatively estimate a decision maker's preferences for a multi-attribute problem. A set of design configurations are systematically created and then ranked by a decision maker based on each configuration's design attributes. Since the ranking of design alternatives can be used to elicit a decision maker's preferences, CVA is considered a decision-making method pertaining to value theory as described [13]. In CVA, the ranking of each design is influenced by the contribution of all system attributes considered, allowing for the estimation of part-worths that represent respondent(s) preferences [14]. These respondents can be customers, producers or decision makers, in the case of a design team conducting the analysis.

In this research, CVA is used to create part-worth plots, based on the design engineer's preferences. As illustrated in the flowchart of Figure 4, CVA starts with the selection of attributes $f_i(X), i = 1, 2, \ldots \ldots k$ that are most relevant to the design problem.

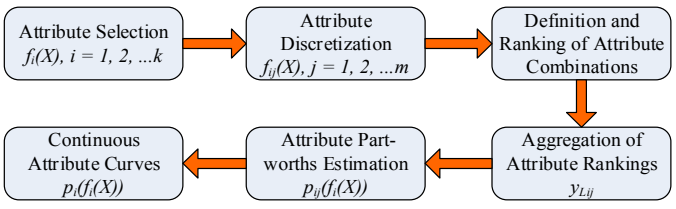

Figure 4: Flowchart for conjoint analysis

For each selected attribute, the expected range is discretized such that $f_{ij}(X), j = 1, 2, \ldots\ldots m$, where m denotes the number of preferred levels. Different attribute combinations can be chosen to represent possible system performance features. It is not always practical to consider a full factorial set of attribute combinations as, in some cases, it can be cumbersome to define and sort the preferences. Thus, fractional factorial designs should be considered [15].

The next step is to rank the combinations so that the rankings reflect user or designer preferences. Several preference aggregation methods exist [11]; the choice of method depends on the nature of the rankings. This work employs the dummy-variable regression technique [16] to estimate attribute part-worths, using ordinary least squares regression analysis. Part-worths are estimated by first normalizing the combination rankings y_N using

$$y_N = \frac{y - y_{min} + 1}{y_{max} - y_{min} + 2} \tag{13}$$

where y is the ranking of each attribute combination and y_{min} and y_{max} are the minimum and maximum rankings respectively. This normalized value is then used to calculate the logit coded ranking value, y_L using:

$$y_L = ln\frac{y_N}{1 - y_N} \tag{14}$$

This recoding performed for each ranking value and used to evaluate the subsequent regression problem. Logit coding [17] is a transformation of the rankings into scaled values that are appropriate for use with Ordinary Least Squares regression methods such as multiple regression. In cases where rankings are used to measure the designer's preferences, logit recoding of the ranking values is required. This is because Ordinary Least Squares regression methods are not appropriate for conjoint data consisting of rank orders due to the difference between the representation of a rating and a ranking. In a rating, the data is scaled so that real differences in combinations are communicated by the arithmetic differences in their value. In other words, the difference between a rating of a 1 and 2 is the same as the difference between a rating of 9 and 10. In rankings, the same assumption cannot be true. For instance, a combination with a ranking of 4 is not necessarily twice as preferred as the combination ranked 2.

Finally, regression analysis is performed and the resulting coefficients are the attribute part-worths p_{ij} that represent preferences for all the selected attribute levels. To normalize the part-worths, zero-centered transformation can be applied to the regression analysis results.

Preference curves for the one-to-one mapping between the discrete attributes and corresponding part-worths can be separately generated for each attribute. To perform optimization, continuous part-worth curves are needed, and can be obtained by piecewise linear interpolation and extrapolation of discrete part-worths curves. With the availability of continuous part-worths $p_1(f_1(X)), p_2(f_2(X)), \ldots . p_k f_k(X)$ for each attribute, the optimization problem is solved using an objective formulation that is based on part-worths.

3.2 OBJECTIVE FUNCTION

In this implementation of CVA, the objective function is formulated as the negative sum of the attribute part-worths such that the optimization objective becomes minimization of this function as follows.

$$\text{Minimize} \quad g(f(X)) = -\sum_{i=1}^{k} p_i(f_i(X)) \tag{15}$$

$$\text{subject to} \quad X_L \le X \le X_U$$

According to the part-worths definition, larger values are more desirable, thus, the negative sign transforms the maximization of part-worths into a minimization problem.

3.3 OPTIMIZATION METHOD

MATLAB's™ gradient-based Sequential Quadratic Programming (SQP) method [18] is used to conduct the optimization. This method requires gradients of only active constraints, allows starting points to be infeasible, and accommodates equality constraints. The task of generating a new point is divided into two parts. The first part is getting the direction d_k and the step size α_k. The new point in the design space is obtained as $x_{k+1} = \alpha_k d_k$. In this method, the direction vector, d_k is obtained by solving the QP sub-problem, shown below.

$$\begin{aligned} &\text{Minimize} && \frac{1}{2} d^T d + \nabla f^T d \\ &\text{Subject to} && \nabla g_i^T d + g_i^T d \le 0 \\ &&& \nabla h_i^T d + g_i^T d \le 0 \\ &&& x^L \le d + x_k \le x^U \end{aligned} \tag{16}$$

where d is the design variable. ∇f, ∇g and ∇h are the gradients of the objective, inequality constraints and equality constraints respectively. Thus d_k, the direction vector, is obtained. Step size, α_k is chosen equal to 0.5^J where J is the first of the integers $q = 1,2,3 \ldots$ for which the following inequality holds:

$$\theta(x_k + 0.5^q d_k) \le \theta(x_k) - \gamma 0.5^q \|d\|_2 \tag{17}$$

where $\theta(x)$ can be used as a descent function. Further details of the method can be seen in [18] and [19].

3.4 UNCERTAINTY AND SENSITIVITY ANALYSES

The Monte Carlo method [20] of performing uncertainty and sensitivity analyses selects a random set of design parameter values drawn from their individual probability distributions. These values are then used in the simulation model to obtain corresponding system output values. This process is repeated many times, each time making sure the output is valid for the chosen parameter values. The result is a probability distribution of system attributes that result from design parameters variations.

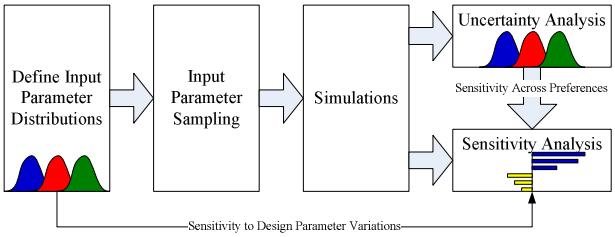

Figure 5: Illustration of the Monte Carlo based Uncertainty and Sensitivity Analysis methodology

3.4.1 UNCERTAINTY ANALYSIS

Uncertainty [21] involves the notion of randomness. If the value of a performance measure varies, and this variation over space and time cannot be predicted with certainty, it is called a random variable. One cannot say with certainty what the value of a random variable will be, but only the likelihood or probability that it will be within some specified range. An uncertainty analysis takes a set of randomly chosen design parameter values and evaluates distributions (or statistical measures) of the resulting outputs [20], [21].

As illustrated in Figure 5, the Monte Carlo-based uncertainty analysis involves the following four steps.

1. Design parameter range and distribution selection: If the analysis is exploratory, rough distribution assumptions may be adequate. In this research, the design vector elements are assigned a normal probability distribution. The normal distribution is chosen because it maximizes the information entropy among all distributions with a known mean and standard deviation [22]. The standard deviations were obtained from statistical data gathered by a shale shaker manufacturer. The data quantifies the previously observed standard deviations of actuator locations as a result of design and manufacturing imprecision.
2. Sample points generation: Too few samples lead to inaccurate outputs and graphs (particularly histogram plots and distributions) that are inconclusive; Too many samples might take a long time to simulate, and it may take even longer to plot graphs, export and analyze the data. Ultimately, the number of samples depends on the required 95% confidence interval around each distribution mean. In this research, 1000 different samples were generated for the Monte Carlo study.
3. Simulation: Model evaluations create a mapping from the parameter space to the attribute space. This mapping is the basis for subsequent uncertainty and sensitivity analysis.
4. Analysis: Finally, model outputs are used as the basis for uncertainty analysis. One way to characterize the uncertainty is with a mean and standard deviation of the system attribute distributions. Performance probability analysis is also used to estimate the probability that the output will meet a specific performance measures / target values.

3.4.2 SENSITIVITY ANALYSIS

Sensitivity analysis [23], [22], [24] aims to describe the extent to which output values are affected by changes in design parameter values. It investigates the effect of design parameters imprecision on the system attributes. Sensitivity studies can provide a general assessment of design parameter importance by evaluating the relative significance of errors in various parameters.

The results of Monte Carlo model evaluations are used as the basis for sensitivity analysis. In this research, the correlation between each design parameter and the system outputs is used as a sensitivity measure. For each design parameter $X(i)$ and attribute $f_j(X)$, the correlation coefficient $r_{X(i),f_j(X)}$ between the design parameter and the attribute is given by

$$r_{X(i),f_j(X)} = \frac{1}{n-1}\left(\frac{\Sigma_{X(i)}\Sigma_{f_j(X)}\left(X(i)-\overline{X(i)}\right)\left(f_j(X)-\overline{f_j(X)}\right)}{\sigma_{X(i)}\sigma_{f_j(X)}}\right) \quad (18)$$

where n is the number of data pairs, $\overline{X(i)}$ and $\overline{f_j(X)}$ are the sample means of all the $X(i)$ and $f_j(X)$ values, respectively; $\sigma_{X(i)}$ and $\sigma_{f_j(X)}$ are the sample standard deviations of all the $\overline{X(i)}$ and $f_j(X)$ values, respectively.

The correlation coefficient is then used as a sensitivity measure that quantifies the magnitude change of the system attributes $f_1(X), f_2(X)$ and $f_3(X)$ per unit change in design parameter values X. It is a measure of the linear relationship strength between two variables. If the relationship between the variables is not linear, then the correlation coefficient does not adequately represent the strength of the relationship between the variables. However, in this application, data samples represent perturbations from the nominal design parameters, the linearity assumption employed in the calculation of the correlation coefficients is considered valid.

Another aspect of sensitivity analysis is performed by analyzing the differences in distributions. The differences in uncertainty behavior between solutions derived from different preferences reflect the system design sensitivity to the designer preferences.

4 SIMULATION

4.1 SIMULATION PARAMETERS

Table 1 shows the physical parameters used for system simulations. All locations are based on the coordinate system defined in Figure 1. The initial actuator locations from which all optimizations start are based on a prototype PVS that was designed prior to the development of the optimization scheme introduced in this paper. The screen basket, disturbance torque and CVA models were simulated using MATLAB.

Table 1: PVS physical parameters

Parameter	Value	Description
L	$2000\ mm$	Screen basket length
M	$2000\ kg$	Screen basket mass
J_z	$140\ kg \cdot m^2$	Screen basket Inertia
m_A	$100\ kg$	Actuator mass
J_A	$1.2\ kg \cdot m^2$	Actuator inertia
ω	$188 \cdot rads^{-1}$	Vibration angular velocity
ρ	$0.675\ kg \cdot m$	Eccentric mass imbalance
$[x_{cg}, y_{cg}]$	$[1090, 535]mm$	Screen basket CG location
$[x_{m1}, y_{m1}]$	$[2000{,}350]\ mm$	Measurement location 1
$[x_{m2}, y_{m2}]$	$[1000{,}350]\ mm$	Measurement location 2
$[x_{m3}, y_{m3}]$	$[0, 350]\ mm$	Measurement location 3
n	3	Number of actuators
$[n_1, n_2, n_3]$	$[-1{,}1{,}-1]$	Actuator rotational direction

4.2 OPTIMIZATION CONSTRAINTS

The design optimization problem was configured as in Equation (15) and the design constraints $\boldsymbol{X}_L$ and $\boldsymbol{X}_U$ were defined as deviations from the initial design point $\boldsymbol{X}_0$.

$\boldsymbol{X}_L$= [-0.100 -0.100 -0.100 -0.250 -0.250 -0.250 -0.0338] m

$\boldsymbol{X}_U$= [0.300 0.300 0.300 0.100 0.100 0.100 0.0338] m

The actuator locations were optimized individually, with no constraint keeping them at fixed relative locations. However, the optimization was configured to eliminate solutions with actuator space overlap, based on the expected actuator space envelopes.

4.3 DESIGNER PREFERENCES

Based on a set of preferences, Conjoint Value Analysis (CVA) was used to generate part-worth curves that are used to formulate the objective function. The optimization was set up such that the resulting solution X indicates deviation of the design vector X from the nominal starting design.

Discretized levels for $f_1(X)$, $f_2(X)$ and $f_3(X)$ were selected as shown in Table 2.

Table 2: Discretized levels for $f_1(X)$, $f_2(X)$ and $f_3(X)$

#	$f_1(X)$ (G's)		#	$f_2(X)$ (Deg.)		#	$f_3(X)$ (Nm)^2
1	0.00		5	-15		9	0
2	0.60		6	0		10	300
3	1.00		7	5		11	600
4	1.50		8	15		12	900

Since there are 64 total combinations, a fractional factorial design of 30 combinations was considered. The designer preferences were selected as shown in Table 3, where the highest rank number reflects the most preferred design alternative.

Figure 6 shows $f_1(X), f_2(X)$ and $f_3(X)$ preference curves for the chosen ranking scheme where high part-worth values represent desirable attribute levels. The $f_2(X)$ curves for preference1 and 2 are identical because the attributes are ranked the same way. Also, the $f_2(X)$ curves show the value of 0 as the most preferred because it means no error.

Table 3: Designer preferences for attribute combinations

Rank	Combination		Rank	Combination	
	Pref. 1	Pref. 2		Pref. 1	Pref. 2
30	1,6,9	1,6,9	15	4,8,10	2,8,12
29	2,6,9	1,6,10	14	2,5,11	3,5,10
28	1,8,9	1,8,9	13	1,8,11	3,8,9
27	2,7,9	1,7,10	12	3,5,11	3,5,11
26	1,5,10	2,5,9	11	2,8,11	3,8,10
25	3,5,9	1,5,11	10	3,7,11	3,7,11
24	2,5,10	2,5,10	9	1,6,12	4,6,9
23	3,6,9	1,6,11	8	4,6,11	3,6,12
22	3,8,9	1,8,11	7	4,7,11	3,7,12
21	1,7,10	2,7,9	6	1,7,12	4,7,9
20	2,7,10	2,7,10	5	2,6,12	4,6,10
19	4,6,9	1,6,12	4	3,6,12	4,6,11
18	4,7,9	1,7,12	3	2,8,12	4,8,10
17	4,8,9	1,8,12	2	3,8,12	4,8,11
16	1,6,11	3,6,9	1	4,5,12	4,5,12

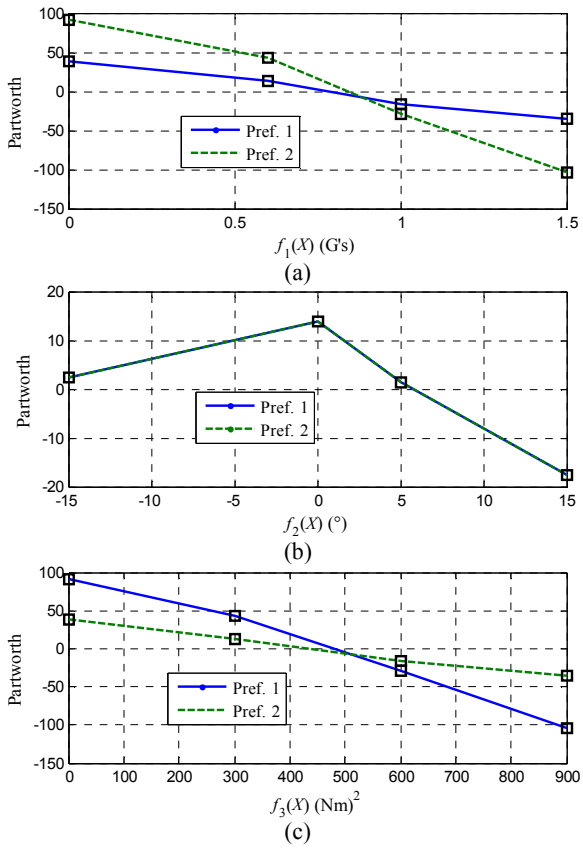

Figure 6: Preference curves for (a) $f_1(X)$, (b) $f_2(X)$ and (c) $f_3(X)$

5 RESULTS AND DISCUSSION

5.1 PVS DESIGN OPTIMIZATION

The respective solutions $\boldsymbol{X}_1$ and $\boldsymbol{X}_2$ based on preferences 1 and 2 were

$\boldsymbol{X}_1$= [0.100 0.350 0.350 -0.177 -0.071 -0.100 -0.0082] m

$\boldsymbol{X}_2$= [0.300 0.300 0.175 -0.219 0.022 -0.196 0.0338] m

where $\boldsymbol{X}_1$ and $\boldsymbol{X}_2$ are the design parameter offsets relative to the initial design point $\boldsymbol{X}_0$.

Figures 7 and 8 show the system vibration performance for profile 1, based on the optimized design vectors $\boldsymbol{X}_1$ and $\boldsymbol{X}_2$.

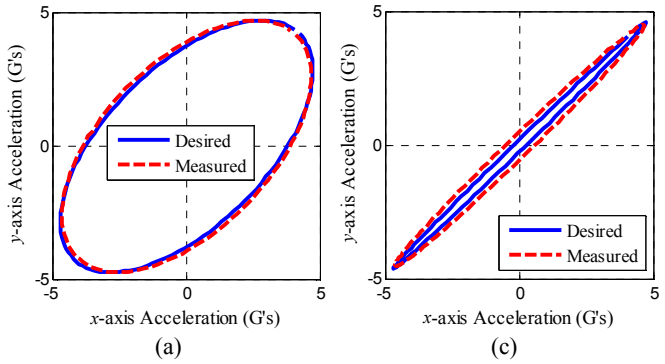

Figure 7: X_1 design performance for a progressive profile (profile 1) at locations (a) 1 and (b) 3

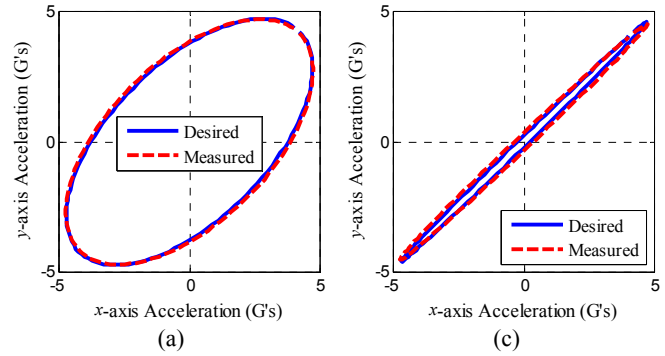

Figure 8: X_2 design performance for a progressive profile (profile 1) at locations (a) 1 and (b) 3

The initial design configuration (an open-loop prototype built before these optimization tools were developed), represented by the design vector X_0, was used as a benchmark for performance and efficiency comparisons. Table 4 shows the attribute percent improvement over the initial design point X_0 across five vibration profiles. Profile 1 is the progressive profile shown in Figure 8 while profiles 2 – 5 represent a mix of uniform elliptical and linear motions with varying acceleration magnitudes. The overall performance shows significant reductions in $f_1(X)$, $f_2(X)$ and $f_3(X)$.

Table 4: Performance improvement across five vibration profiles

Profile	Percent Improvement (%)					
	$f_1(X)$		$f_2(X)$		$f_3(X)$	
	X_1	X_2	X_1	X_2	X_1	X_2
1	86.1	94.4	97.6	95.6	98.8	79.5
2	8.0	14.2	62.4	78.6	2.1	-0.7
3	53.6	66.5	83.5	87.6	51.3	24.7
4	51.9	65.9	54.7	64.5	38.1	23.0
5	3.7	12.1	67.5	71.4	50.0	5.9

The performance results shown in Figure 7, Figure 8 and Table 4 demonstrate how preferences can influence design and performance. Preference 1 favored lower values of $f_3(X)$, while preference 2 was weighted to minimize $f_1(X)$. This is consistent with the observed results where Preference 1 yielded a more 'efficient' design while the preference 2-based design provided better "performance" according to the system attribute definitions.

5.2 PVS DESIGN UNCERTAINTY AND SENSITIVITY

The specified design parameter means are based on the nominal solutions X_1 and X_2 while the standard deviations were chosen based on an insight in the manufacturing variability that can affect the design parameters. Table 5 shows the means and standard deviations of the resulting attribute outputs.

Table 5: Monte Carlo attribute distributions

		$f_1(X)$	$f_2(X)$	$f_3(X)$
Means	μ_{X_1}(Pref. 1)	0.15	0.44	22.63
	μ_{X_2}(Pref. 2)	0.06	0.53	101.27
Standard Deviations	σ_{X_1}(Pref. 1)	0.02	0.22	21.97
	σ_{X_2}(Pref. 2)	0.01	0.10	19.33

The mean of 1000 generated $f_1(X)$, $f_2(X)$ and $f_3(X)$ values are shown in Table 5. However, a different set of random values would have generated a different set of attribute means. Thus, it is appropriate to estimate the standard error SE, of this average. For a sample size n, the standard error is given by

$$SE = \frac{\sigma}{\sqrt{n}} \tag{19}$$

where σ is the standard deviation of the sample population.

From the central limit theorem [25], the average of a large number of independent values should have a nearly normal distribution. Thus, 95% of the time, the true mean of the attributes should be in the interval

$$\mu \pm 1.96(SE) \tag{20}$$

resulting in the following ranges for the means.

Table 6: Statistical ranges for the attribute means

	$f_1(X)$	$f_2(X)$	$f_3(X)$
X_1	0.15 ± 0.001	0.44 ± 0.014	22.63 ± 1.362
X_2	0.06 ± 0.001	0.53 ± 0.006	101.27 ± 1.198

This level of uncertainty (≤ 6% variation) in the generated attribute means reflects that the sample size of 1000 values is sufficient for this study.

The uncertainty analyses were performed for two alternative designs, whose resulting attribute distributions are shown in Figure 9. Figure 9(a)-(c) shows the generated attribute distribution. The vertical marks show the attribute values evaluated using the design parameter distribution means. One can see that, given the estimated levels of uncertainty, the $f_1(X)$, $f_2(X)$ and $f_3(X)$ respective ranges are [0.12, 0.24], [0.1 1.6] and [0, 100] for the preference 1 based analysis and [0.05, 0.1], [0.1 0.9] and [70, 160] for the preference 2- based analysis.

The figure illustrates the extent to which the parameter imprecisions can affect the attributes. This gives an overview of the potential system costs in terms of the system attribute degradation. Based on the standard deviation and the overall shape of the distributions, the design's proximity to discontinuous regions can be identified. Distributions that are generally smooth indicate the stability of the region in which the design is located. As an example, Figure 9(b) shows two $f_2(X)$ values that dominate the localized region of the preference 2-based design. Also, the deviation of the attribute sample means from the ideal design point (red bars in Figure 9(a)-(c)) indicate that the presence of uncertainty almost guarantees that the system will mostly operate away from the ideal design point.

Figure 9(d)-(f) shows the empirical cumulative distribution functions (ecdf) for the system attributes as functions of attribute thresholds. These functions reflect the probability of the system meeting or exceeding the chosen attribute performance thresholds. As an example, the red lines illustrate what the probability of compliance would be if the design acceptance thresholds are set to (a) $f_1(X) = 0.20$ Gs, $f_2(X) = 1.0$ degrees and $f_3(X) = 100$ (Nm)^2. When used with performance thresholds, these plots can be used to quantify the expected system robustness by providing the probability that the system will meet a specific attribute target for any assumed design imprecision. These plots can be incorporated into the product design process to aid the decision making process.

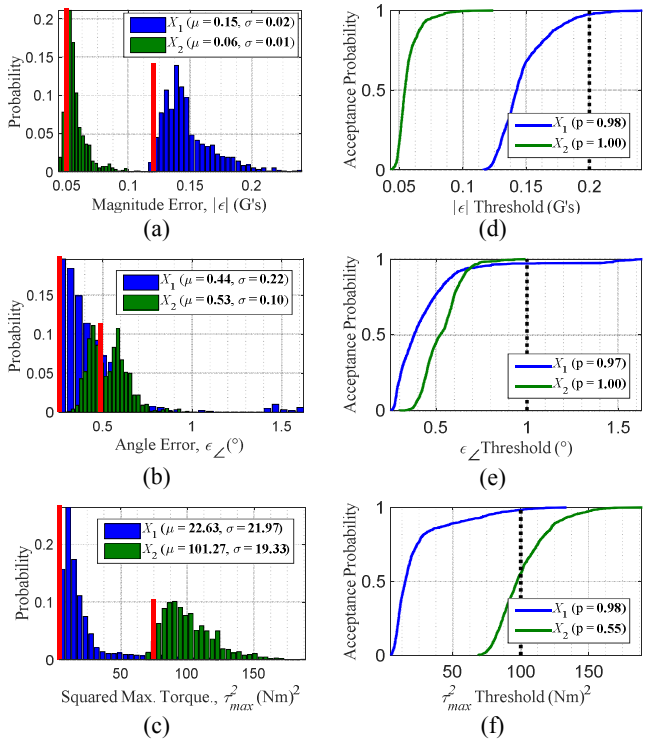

Figure 9: (a)-(c) Attribute distributions from Monte-Carlo analysis. The red bars show the attribute values evaluated using the design parameter distribution means. (d)-(f) Probability of acceptance as a function of attribute thresholds. The dotted lines illustrate the probability of acceptance with performance thresholds set to $f_1(X) = 0.20$ Gs, $f_2(X) = 1.0^o$ and $f_3(X) = 100$ (Nm)^2

Figure 10 illustrates the correlation coefficients between the attributes and each of the design vector elements for both (a)-(c) preference 1 and (d)-(f) preference 2 designs. As the figure shows, the correlation coefficients magnitudes do not offer any conclusive trends about the relative importance of the design elements. While the individual design parameters can affect attributes differently, their overall impact on the entire system can be considered to be of similar magnitude. This can be interpreted as uniform importance of the design parameters. This is consistent with the observation that PVS performance is as much dependent on the actuator absolute locations as is it on the relative locations.

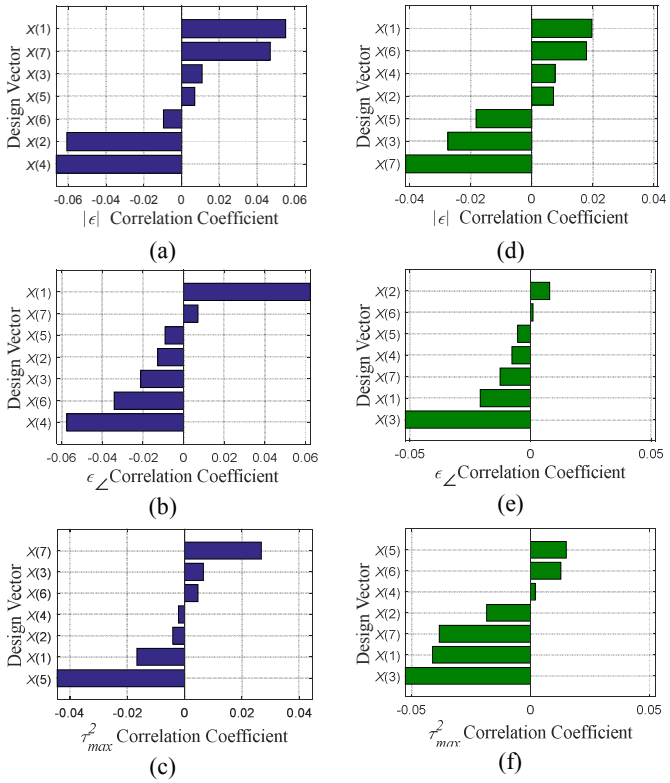

Figure 10: Correlation coefficients between system attributes and (a)-(c) X_1design vector elements (d)-(f) X_2 design vector elements

6 CONCLUSION

The CVA-based optimization approach effectively quantified and optimized preference-based trade-offs in the design process, and yielded performance improvements in all system attributes across all simulated vibration profiles.

This paper presented uncertainty and sensitivity analyses in the context of the prescribed vibration system. The presented methodology aims at helping the designer make informed decisions so that small variations in design parameters and/or manufacturing precision do not impact the decisions themselves. It identifies the extent to which system attributes are sensitive to the specification of the design parameter distributions, as a way to quantify the design risk and robustness. If it appears that reducing system uncertainty is worthwhile, then one should consider how best to do it. If it involves obtaining additional information, then it is clear that the value of this additional information, however measured, should exceed the cost of obtaining it. The value of such information is the increase in system performance or the reduction in its variance.

Future work includes developing a framework for using uncertainty and sensitivity studies to guide design decisions without the need for accurate system models.

7 REFERENCES

[1] B. Malinga and G. Buckner, "Design Optimization of a Prescribed Vibration System using Conjoint Value Analysis," *Engineering Optimization,* 2016.

[2] M. Sabeghi, W. Smith, J. Allen and F. Mistree, "Solution Space Exploration in Model-Based Realization of Engineered Systems," in *International Design Engineering Technical Conferences and Computers and Information in Engineering Conference*, Boston, Massachusetts, 2015.

[3] K. A. Von Hagel and S. M. Ferguson, "Effect of Expert Data Variability in the Change Prediction Method," in *International Design Engineering Technical Conferences and Computers and Information in Engineering Conference*, Anaheim, California, 2014.

[4] G. A. Hazelrigg, "A Framework for Decision-Based Engineering Design," *Journal of,* vol. 120, no. 4, pp. 653-658, 1998.

[5] J. W. Herrmann, "Decision-Based Design Processes," University of Maryland, College Park, MD, 2008.

[6] K. C. W. Lewis and L. C. Schmidt, Decision Making in Engineering Design, New York: ASME Press, 2006.

[7] M. G. Stewart, D. V. Rosowsky and D. V. Val, "Reliability-Based Bridge Assessment Using Risk-Ranking Decision Analysis," *Structural Safety,* vol. 23, no. 4, pp. 397-405, 2001.

[8] D. D. Leon, "Reliability-Based Decision Making for Steel Connections on Seismic Zones," in *Joint International Conference on Computing and Decision Making in Civil and Building Engineering*, Montreal, Canada, 2006.

[9] S. Rangavajhala and A. Messac, "Designer's Preferences Regarding Equality Constraints in Robust Design Optimization," *Structural and Multidisciplinary Optimization,* p. 19, 2008.

[10] S.-K. Choi, R. V. Grandhi and R. A. Canfield, Reliability-Based Structural Design, London, England: Springer-Verlag London, 2007.

[11] P. E. Green and V. Srinivasan, "Conjoint analysis in marketing : New developments with implications for research and practice.," *Journal of Marketing,* vol. 54, pp. 3-19, 1990.

[12] American Association of Drilling Engineers, "Shale Shaker and Drilling Fluids Systems: Techniques and Technology for Improving Solids Control Management," Gulf Professional Publishing, 1999.

[13] R. T. Clemen, Making Hard Decisions: An Introduction to Decision Analysis, South-Western College Pub, 2000.

[14] T. Reutterer and H. W. Kotzab, "The use of conjoint analysis for measuring preferences in supply chain design.," *Industrial Marketing Management,* vol. 9, pp. 27-35, 1999.

[15] W. H. Kuhfeld, R. D. Tobais and M. Garratt, "Efficient experimental design with marketing research applications," *Journal of Marketing Research,* vol. 31, pp. 545-557, 1994.

[16] Sawtooth-Software, *SMRT Application Help and Documentation,* Sequim, WA: Sawtooth Software, Inc.

[17] H. Theil, "A Multinomial Extension of the Linear Logit Model," *International Economic Review,* vol. 14, no. 10, pp. 1079-1083, 1969.

[18] Mathworks-Incorporated, "Optimization Toolbox Users Guide," Mathworks Incorporated, Natick, MA, 2014.

[19] A. D. a. C. T. R. Belugundu, Optimization Concepts and Applications in Engineering., New Jersey: Prentice-Hall Inc., 1999.

[20] I. M. Sobol, A Primer for the Monte Carlo Method, Crc Press, 1994.

[21] R. Cooke, Experts in Uncertainty: Opinion and Subjective Probability in Science, Oxford University Press, 1991.

[22] SimLab, "Uncertainty and Sensitivity Analysis," SimLab, [Online]. Available: http://simlab.jrc.ec.europa.eu. [Accessed January 2016].

[23] H. Frey and S. Patil, "Identification and review of sensitivity analysis methods," *Risk Analysis,* vol. 22, no. 3, pp. 553-578, 2002.

[24] A. Saltelli, K. Chan and E. Scott, Sensitivity analysis, Chichester, UK: Wiley, 2000.

[25] W. Feller, "The fundamental limit theorems in probability," *Bulletin of the American Mathematical Society,* vol. 51, pp. 800-832, 1945.